Fiber Bragg gratings operating across arbitrary wavelength ranges

Yosuke Mizuno,[1,*] Naoki Motoishi,[1,2] Kohei Noda,[1,2] Antreas Theodosiou,[3]
Kyriacos Kalli,[3] Heeyoung Lee,[4] Kentaro Nakamura,[2] and Marcelo A. Soto[5]

[1] *Faculty of Engineering, Yokohama National University, Yokohama 240-8501, Japan*

[2] *Institute of Innovative Research, Tokyo Institute of Technology, Yokohama 226-8503, Japan*

[3] *Photonics and Optical Sensors Research Laboratory, Cyprus University of Technology, Limassol 3036, Cyprus*

[4] *College of Engineering, Shibaura Institute of Technology, Tokyo 135-8548, Japan*

[5] *Department of Electronics Engineering, Universidad Técnica Federico Santa María, Valparaíso 2390123, Chile*

[*]E-mail: mizuno-yosuke-rg@ynu.ac.jp

Abstract: We demonstrate that fiber Bragg gratings in polymer optical fibers can lead to reflection peaks in any wavelength range when exciting high-order propagation modes, which can enhance the design of sensing systems for specific applications.

Fiber Bragg gratings (FBGs) are distributed reflectors inscribed in a short segment of an optical fiber to reflect particular wavelengths of light. They are used for a wide range of practical applications in communication and sensing and are currently regarded as one of the most fundamental optical devices.[1–5] When inscribed in single-mode fibers (SMFs), FBGs reflect only a single wavelength of light, known as Bragg wavelength $\lambda_B = 2\,n_{\text{eff}}\,\Lambda$, where n_{eff} is the effective refractive index of the fiber core and Λ is the grating pitch. Higher-order diffraction reflections also occur at submultiple wavelengths. However, when inscribed in multimode fibers (MMFs),[6–14] FBGs show multiple reflection peaks around the fundamental Bragg peak. These multiple peaks originate from the coupling between different linearly polarized (LP) modes and can be utilized for discriminative sensing of distinct physical parameters. However, such multiple peaks appear only within limited wavelength ranges around the fundamental Bragg peak. If such spectral peaks are induced across all wavelength ranges, FBG sensing using light sources at arbitrary operating wavelengths will be feasible, increasing the flexibility in selecting optical devices and benefiting not only standard wide-

range detection of Bragg wavelengths but also spectral-slope-assisted vibration sensing.

In this work, we demonstrate that multiple reflected Bragg peaks can be induced in any wavelength range in a multimode polymer optical fiber (POF) by intentionally suppressing the fundamental LP mode and exciting higher-order modes. Preliminary experimental results prove that this previously unreported behavior is specific to FBGs inscribed in POFs. The origin of multiple spectral peaks in POF-FBGs is presumably due to the eventual partial FBG inscription in the POF core resulting from plane-by-plane femtosecond-laser inscription. Through experimental analysis, results also clearly verify that the induced behavior is caused by the multimode response of the FBG (with suppressed fundamental mode) and not by Fabry-Perot or multimodal interference. In addition to classical wavelength-based FBG sensing, the experiments also confirm the potential for spectral-slope-assisted vibration sensing in arbitrary wavelength ranges using this method.

An FBG is inscribed in a 1.4 m-long perfluorinated graded-index (GI) POF,[15–23] which consists of a 50 μm diameter core (refractive index: ~1.345), a 70 μm cladding, and a 490 μm overcladding. The core and cladding are made of doped and undoped amorphous fluoropolymer, respectively, while the overcladding is composed of polycarbonate. The optical propagation loss is ~0.25 dB/m at 1550 nm. A 2 mm-long FBG is inscribed in the middle of this POF directly, without removing the overcladding, using a femtosecond laser at 517 nm with 220 fs pulses, a 1 kHz repetition rate, and ~100 nJ pulse energy. The POF is placed on a two-axis translation system, and a long-working-distance objective (x50) on the third axis is used to focus the laser beam onto the POF. By synchronizing the laser pulse repetition rate and the stage motion, a plane-by-plane FBG is inscribed with a pitch of 2.32 μm, corresponding to the 4th-order Bragg peak at ~1560 nm.

The experimental setup for measuring the Bragg wavelengths of the POF-FBG is depicted in Fig. 1(a). All optical paths, except for the POF, are silica SMFs. Here, the reflected spectrum is observed, because the transmitted spectrum is largely influenced by multimodal interference caused by the single-mode-multimode-single-mode (SMS) structure.[24–29] The POF has flatly polished ends, one of which is connected to a silica SMF by butt-coupling[30] and the other left open. The output from a supercontinuum source, the spectrum of which is shown in Fig. 1(b), is injected into the POF. The reflected light is directed to an optical spectrum analyzer (OSA) via an optical circulator, which has an operating wavelength range around 1550 nm. Strains from 0 to 0.4 % are applied to a 1.0 m-long POF section (with the FBG in the middle) fixed on translation stages.

Figure 2 compares the FBG-reflected spectra measured when the fiber cores are aligned

(blue) and misaligned (orange) at the SMF-POF boundary. With aligned cores, clear FBG-reflected peaks are observed at 1248 and 1560 nm, corresponding to the 5th and 4th Bragg diffraction orders, respectively. The 6th-order Bragg peak at 1043 nm cannot be seen because of the wavelength-dependent loss of the circulator. When the SMF and POF cores are misaligned, the clean fundamental and high-order diffraction reflection peaks disappear and are replaced by numerous peaks across a wide wavelength range. These peaks are not perfectly defined in Fig. 2 (orange) due to the limited bandwidth resolution used in this measurement (details are later shown in Fig. 3). In spectra reflected from silica multimode FBGs, some small peaks sometimes appear around the fundamental Bragg reflection peak,[6–14] but no reflections are observed at other wavelengths. Thus, the generation of multiple FBG reflection peaks over an ultrawide wavelength range is a unique behavior of the POF-FBG, presumably caused by eventual partial grating inscription in the POF core, resulting from the plane-by-plane femtosecond-laser inscription method used.

Magnified views of the POF-FBG-reflected spectrum (when using misaligned cores) around 1300, 1400, and 1500 nm are shown in Figs. 3(a)–3(c), respectively. Multiple peaks in an extremely wide spectral range are observed with narrow spectral spacings, though their isolations are small (roughly 5 dB). The strain dependence of a random spectral peak around each spectral window is shown in Figs. 4(a)–4(c). Each peak redshifts linearly with increasing strain, with sensitivities of 11.36, 11.79, and 13.12 nm/%, respectively. These values are consistent with the order of magnitude reported for a perfluorinated GI-POF-FBG.[16] In this setup, which forms a folded SMS structure, multiple spectral peaks could also be generated by multimodal interference,[24–29] but such peaks are much broader (width: over tens of nanometers) and their strain coefficients at telecommunication wavelengths are of the order of 1000 nm/%; in addition, their signs are negative.[24] Thus, the multiple induced peaks are not due to modal interference, though the strain dependence of the peak power may be attributed to this effect. In addition, a Fabry-Perot cavity[31–33] is not formed in the POF, considering the high one-cycle optical loss. A preliminary analysis by extrapolation of the strain coefficient suggests a linear behavior versus wavelength, with a fitted first-order line crossing the origin, further confirming that the observed peaks are induced by the FBG inscription process with core misalignment. Note that our previous characterization of the strain and temperature dependencies of the spectral peak wavelengths (with aligned cores)[16] indicates a significant difference in their behaviors with respect to wavelength between the two. In particular, in such cases, we observed that while the strain coefficients of the peaks were almost identical within a limited wavelength range, the temperature coefficients were

largely different even within the same range. The experimental data reported in this work with misaligned cores supports the same behavior on strain. However, at this stage, we cannot assume that the temperature dependence of the spectral peak wavelengths with misaligned cores will behave the same as the strain dependence. Further studies are required to investigate this point.

An interesting feature of the created FBG reflections peaks is that, besides conventional FBG-based sensing, the multiple peaks can be exploited for spectral-slope-assisted vibration sensing using an arbitrary wavelength range, despite their small spectral separation. To verify this, ~200 με static strain is first applied to the POF-FBG, followed by ~130 με dynamic strain at 50 Hz. Figures 5(a)–5(c) show the dynamic strain measured using the linear regions of the spectral peaks around 1300, 1400, and 1500 nm, respectively. These results confirm that the applied dynamic strain can be properly detected at all three wavelengths. This highlights the capability of the multiple created peaks to perform sensing at any desired wavelength within a very broad spectral range.

In conclusion, we have reported the ability to generate multiple FBG-reflected peaks over an ultra-broadband spectral range by promoting the excitation of higher-order LP modes in a multimode POF. This previously unreported behavior is unique to POF-FBGs. While the phenomenon is presumably attributed to the response of the femtosecond-laser inscribed FBG to multiple LP modes propagating in the POF, the multiple spectral reflections cannot be explained by Fabry-Perot or multimodal interference. This can be verified by the strain sensitivity, which matches the order of magnitude reported for GI-POF-FBGs and significantly differs from the sensitivity reported for multimode interference (approximately –1000 nm/%). Note that the objective of this Letter is to report on the presence of this unexpected and unreported behavior leading to multiple spectral peaks by clear and demonstrative preliminary results. However, a thorough investigation is still required to find conclusive proofs of the physical causes underlying behind this effect. We believe that this newly reported POF-FBG behavior can provide flexibility in selecting optical devices for the development of FBG sensing systems at any desired wavelength.

Acknowledgments

References

1) R. Kashyap, *Fiber Bragg Gratings* (New York: Academic, 1999).

2) J. Bonefacino, H.-Y. Tam, T. S. Glen, X. Cheng, C.-F. J. Pun, J. Wang, P.-H. Lee, M.-L. V. Tse, and S. T. Boles, Light: Sci. Appl. **7**, 17161 (2018).

3) S. Loranger, V. Lambin-Iezzi, and R. Kashyap, Optica **4**, 1143 (2017).

4) L. A. Blanquer, F. Marchini, J. R. Seitz, N. Daher, F. Bétermier, J. Huang, C. Gervillié, and J.-M. Tarascon, Nat. Commun. **13**, 1153 (2022).

5) L. Massari, G. Fransvea, J. D'Abbraccio, M. Filosa, G. Terruso, A. Aliperta, G. D'Alesio, M. Zaltieri, E. Schena, E. Palermo, E. Sinibaldi, and C. M. Oddo, Nat. Mach. Intell. **4**, 425 (2022).

6) C. Lu and Y. Cui, J. Lightwave Technol. **24**, 598 (2006).

7) M. J. Schmid and M. S. Müller, Opt. Express **23**, 8087 (2015).

8) Y.-G. Nan, J. Pan, F. Liu, X. Hu, and P. Mégret, J. Lightwave Technol., doi: 10.1109/JLT.2022.3228506.

9) D. Ganziy, O. Jespersen, G. Woyessa, B. Rose, and O. Bang, Appl. Opt. **54**, 5657 (2015).

10) M. Raguse, S. Klein, P. Baer, M. Giesberts, M. Traub, and H.-D. Hoffmann, Opt. Continuum **1**, 965 (2022).

11) Z. Liu, L. Zhu, L. Lu, C. Shangguan, D. Zhang, and J. Wang, Instrum. Sci. Technol. **49**, 457 (2021).

12) X. Dong, L. Zeng, D. Chu, and X. Sun, Sensors **21**, 5938 (2021).

13) Q. Wang, D. N. Wang, and H. Zhang, Opt. Lett. **44**, 2693 (2019).

14) T. Ayupova, M. Sypabekova, C. Molardi, A. Bekmurzayeva, M. Shaimerdenova, K. Dukenbayev, and D. Tosi, Sensors **19**, 39 (2019.)

15) Y. Koike and M. Asai, NPG Asia Mater. **1**, 22 (2009).

16) Y. Mizuno, R. Ishikawa, H. Lee, A. Theodosiou, K. Kalli, and K. Nakamura, IEEE Sens. J. **19**, 4458 (2019).

17) A. Lacraz, M. Polis, A. Theodosiou, C. Koutsides, and K. Kalli, IEEE Photonics Technol. Lett. **27**, 693 (2015).

18) Y. Mizuno, S. Liehr, A. Theodosiou, K. Kalli, H. Lee, and K. Nakamura, Photonics Res. **9**, 1719 (2021).

19) C. Broadway, R. Min, A. G. Leal-Junior, C. Marques, and C. Caucheteur, J. Lightwave Technol. **37**, 2605 (2019).

20) Y. Mizuno, T. Ma, R. Ishikawa, H. Lee, A. Theodosiou, K. Kalli, and K. Nakamura, Appl. Phys. Express **12**, 082007 (2019).

21) D. Webb, Meas. Sci. Technol. **26**, 092004 (2015).

22) K. Noda, H. Lee, S. Watanabe, K. Nakamura, and Y. Mizuno, Appl. Phys. Express **15**, 122005 (2022).

23) K. Wang, Y. Mizuno, K. Kishizawa, Y. Toyoda, H. Lee, K. Ichige, W. Kurz, X. Dong, M. Jakobi, and A. W. Koch, Jpn. J. Appl. Phys. **61**, 118001 (2022).

24) Y. Mizuno, G. Numata, T. Kawa, H. Lee, N. Hayashi, and K. Nakamura, IEICE Trans.

Electron. **E101-C**, 602 (2018).

25) G. Numata, N. Hayashi, Y. Mizuno, and K. Nakamura, IEEE Photonics J. **6**, 6802306 (2014).

26) G. Numata, N. Hayashi, Y. Mizuno, and K. Nakamura, Appl. Phys. Express **8**, 072502 (2015).

27) K. Wang, Y. Mizuno, X. Su, X. Dong, W. Kurz, M. Fink, H. Lee, M. Jakobi, and A. W. Koch, Appl. Phys. Express **16**, 012003 (2023).

28) K. Toda, K. Kishizawa, Y. Toyoda, K. Noda, H. Lee, K. Nakamura, K. Ichige, and Y. Mizuno, Appl. Phys. Express **15**, 072002 (2022).

29) J. R. Guzmán-Sepúlveda, R. Guzmán-Cabrera, and A. A. Castillo-Guzmán, Sensors **21**, 1862 (2021).

30) Y. Mizuno and K. Nakamura, Appl. Phys. Lett. **97**, 021103 (2010).

31) T. Yoshino, K. Kurosawa, K. Itoh, and T. Ose, IEEE Trans. Microwave Theory Tech. **30**, 1612 (1982)

32) S.-M. Tseng and C.-L. Chen, Appl. Opt. **27**, 547 (1988).

33) T. K. Gangopadhyay, Sens. Actuators A: Phys. **113**, 20 (2004).

Figure Captions

Fig. 1. (Color online) (a) Experimental setup. (b) Measured emission spectrum of the supercontinuum source.

Fig. 2. (Color online) Reflection spectra of an FBG inscribed in a POF, when the fiber cores are aligned (blue) and misaligned (orange).

Fig. 3. (Color online) Reflected spectra magnified around (a) 1300, (b) 1400, and (c) 1500 nm.

Fig. 4. (Color online) Strain dependence of one of the spectral peaks around (a) 1300, (b) 1400, and (c) 1500 nm.

Fig. 5. (Color online) Dynamic strain measured using the slope of different peaks around (a) 1300, (b) 1400, and (c) 1500 nm.
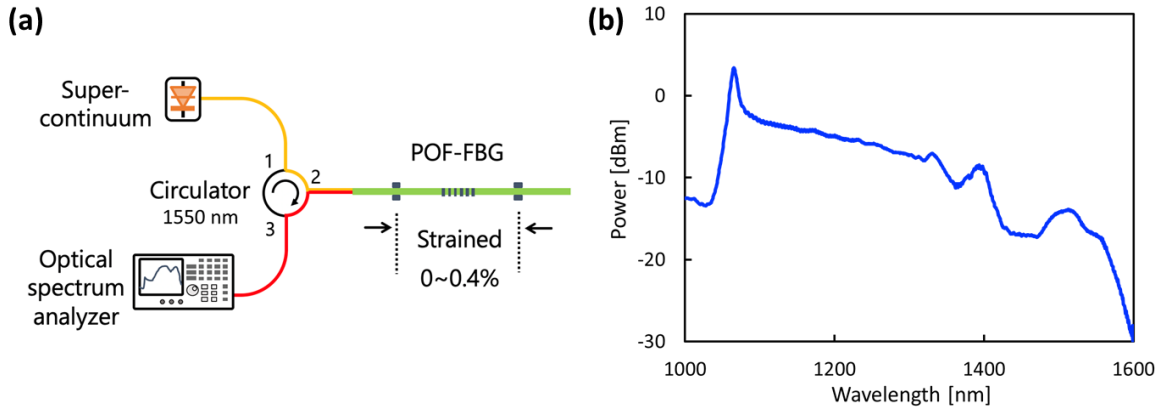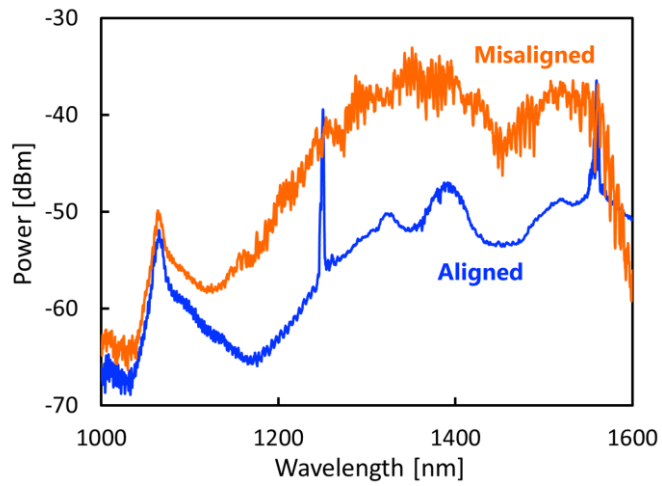
Figures

Fig. 1.

(a)
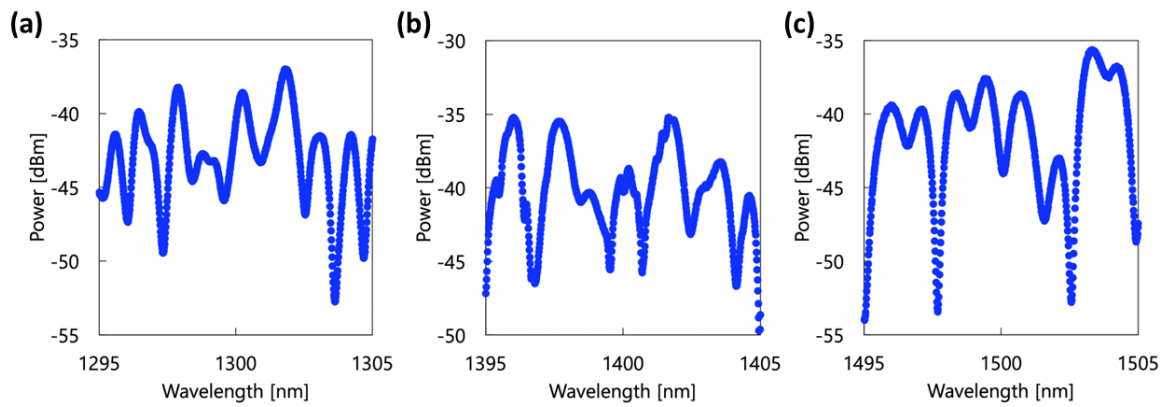

(b)

Fig. 2.

Fig. 3

(a)

(b)

(c)

Fig. 4

Fig. 5